J. Earth Syst. Sci. (2020)129 55
https://doi.org/10.1007/s12040-019-1319-y

GIS-based pre- and post-earthquake landslide susceptibility zonation with reference to 1999 Chamoli earthquake

Sangeeta[1], Bal Krishna Maheshwari[2,*] and Debi Prasanna Kanungo[3]

[1]*Centre of Excellence in Disaster Mitigation and Management (CoEDMM), Indian Institute of Technology, Roorkee, India.*
[2]*Department of Earthquake Engineering, Indian Institute of Technology, Roorkee, India.*
[3]*CSIR–Central Building Research Institute (CBRI), Roorkee, India.*
**Corresponding author. e-mail: bkmahfeq@iitr.ac.in*

MS received 5 July 2019; revised 4 September 2019; accepted 19 October 2019

Landslides induced due to monsoon rainfall and earthquakes are very common phenomena in Uttarakhand Himalayas of India. For example, many such landslides got induced and reactivated by the 1999 Chamoli earthquake. In view of above, authors have made an attempt to prepare pre- and post-earthquake landslide susceptibility zonation (LSZ) maps for a part of Chamoli district, Uttarakhand, India. The novelty of this work lies in producing an LSZ map considering peak ground acceleration (PGA) as one of the controlling factors for earthquake-induced landslide occurrences and validating the LSZ map with the post-earthquake landslide inventory. For this purpose, a spatial database of seven controlling factors, i.e., slope angle, slope aspect, slope curvature, geology, distance to drainage, normalized difference vegetation index (NDVI) and peak ground acceleration (PGA) was prepared in Geographic Information System (GIS). Then, relative frequency ratio (RFR) method was adopted for the LSZ maps. The landslide inventory of 276 landslides (220 pre-earthquake and 56 post-earthquake landslides) was prepared for the study area. Firstly, an LSZ map was generated using six controlling factors excluding PGA and the pre-earthquake landslide inventory (Case I). In another attempt, the LSZ map is prepared using seven controlling factors including PGA and pre-earthquake landslide inventory to examine the influence of seismic parameter (PGA) in landslide susceptibility assessment (Case II). Subsequently, pre- and post-earthquake landslide inventory along with seven controlling factors were used to construct another LSZ map (Case III). Finally, these three LSZ maps were validated and compared with the training and testing data. In this study, a spatial predictive model for earthquake-induced landslide is developed.

Keywords. Earthquake-induced landslide; PGA; landslide susceptibility zonation; relative frequency ratio; GIS.

1. Introduction

Landslide, a very common natural hazard, is recurrently happening in the hilly areas causing extensive causalities and property damage. Therefore, an appropriate landslide hazard analysis is required to reduce such damage. Landslide hazard zonation (LHZ) mapping is defined as the classification of land into homogeneous units and weighing them according to the probability of occurrence of landslides (Varnes 1984). The aim of LHZ mapping (needed for risk assessment) is to

Published online: 22 January 2020

determine the spatial and temporal extent of landslide hazards. Landslide susceptibility zoning involves the spatial distribution and rating of the terrain units (Fell *et al.* 2008). Present study deals with spatial prediction of probable locations of future landslides and thus covers landslide susceptibility zonation (LSZ) mapping.

Landslide hazard assessment requires the integration and analysis of topographical, hydrological, vegetation cover, geological, and seismic conditions along with the existing landslide inventory. In the last few decades, Geographic Information System (GIS) has contributed immensely in the field of disaster. Many researchers use GIS as a tool to analyze landslide hazard (Sarkar and Kanungo 2004; Lee and Evangelista 2006; Wang *et al.* 2015; Abou-Jaoude *et al.* 2016). Various methods have been adopted by researchers in the Himalayan region (Kanungo *et al.* 2006; Pradhan *et al.* 2006; Champati *et al.* 2007; Kumar and Anbalagan 2019).

It is widely recognized that earthquake-induced landslides often cause extensive causalities and economic losses. Earthquake-induced landslide hazard zonation has attracted much attention. Research reported for earthquake-induced landslide hazard assessment in last two decades is summarized in table 1 and classified based on seismic parameter. It can be observed from table 1 that so far no hazard assessment study has been performed for Indian Himalayan region related to earthquake-induced landslides. Umar *et al.* (2014) and Tanoli *et al.* (2017) considered earthquake-induced landslide susceptibility mapping using frequency ratio (FR) method for Indonesia and Nepal region respectively. On the similar line, the present study also used frequency ratio method. In this work, effect of seismic parameter as well as effect of pre-earthquake and earthquake-induced landslide inventory on LSZ has been studied. Based on this comprehensive analysis, a predictive model is proposed, which could be used in the absence of earthquake-induced landslide inventory.

In past three decades (1990–2019), two severe earthquakes, i.e., Uttarkashi earthquake (1991) and Chamoli earthquake (1999) were witnessed by Uttarakhand state. According to BIS (2016), the present study area falls in seismic zone V.

Few researchers (Saha *et al.* 2005; Chauhan *et al.* 2010; Kundu *et al.* 2013; Sarkar *et al.* 2015) worked for LSZ mapping of the Chamoli region. However, their studies were limited to incorporation of static factors only and have not considered the seismic factor. Chauhan *et al.* (2010) and Kundu *et al.* (2013) carried out an LSZ mapping based on remote sensing (RS) and GIS using logistic regression (LR) model. Saha *et al.* (2005) applied landslide nominal susceptibility factor (LNSF) and information value (InfoVal) methods for LSZ mapping. Sarkar *et al.* (2015) defined a landslide intensity scale for the Uttarakhand region. The literature shows that Chamoli district has not been studied for earthquake-induced landslide hazard and seismic factor has not been considered in sensitivity analysis. Major research gap for this seismically active region is the integration of an external triggering parameter, i.e., seismicity for LSZ studies.

Currently, statistical techniques are widely used for landslide hazard assessment. It is a quantitative approach for producing reliable outcomes. Various approaches have been adopted by applying statistical techniques. These methods can broadly be classified into three types: bivariate, multivariate and probabilistic prediction models. Bivariate statistical models (Budimir *et al.* 2015; Hungr 2016; Shrestha *et al.* 2018), multivariate models (Tanoli *et al.* 2017) and probabilistic prediction

Table 1. *Recent research in earthquake-induced landslide hazard/susceptibility assessment.*

	Method		
Seismic parameter	Probabilistic approach	Deterministic approach	Statistical approach
Arias intensity	Song *et al.* (2012)		Lee *et al.* (2008)
Newmark's model	Refice and Capolongo (2002), Gaudio *et al.* (2003), Chousianitis *et al.* (2016)	Bojadjieva *et al.* (2018), James and Sitharam (2014)	
Shake map, shake intensity			Aghda and Bagheri (2015), Miles and Keefer (2009)
Peak ground acceleration		Liu *et al.* (2018)	Lee and Evangelista (2006), Umar *et al.* (2014), Tanoli *et al.* (2017), Sangeeta and Maheshwari (2019)

models (Gaudio *et al.* 2003) have been implemented for the analysis of landslide susceptibility zonation around the globe. Other than these methods, few studies on distribution free analysis such as artificial neural network (ANN) models (Lee and Evangelista 2006), fuzzy set based models (Kanungo *et al.* 2006; Miles and Keefer 2009), and neuro-fuzzy models (Aghdam *et al.* 2017) have been studied for LSZ studies. Wu (2016) and Ding *et al.* (2017) performed a comparison and applicability of landslide susceptibility models and their results shows that FR gives higher prediction rate and accuracy. Therefore, FR model has been adopted in the study area.

The primary objective of this work is to generate a landslide susceptibility zonation (LSZ) map based on pre- and post-earthquake landslide events for a part of Chamoli district, which lies in a very active seismic zone (V). Presented model incorporates inherent parameters along with external parameter (seismicity). Effect of the seismic parameter on landslide susceptibility assessment is examined. Based on this, an earthquake-induced landslide predictive model has been proposed.

It shall be noted that no work has been conducted in the study area related to earthquake-induced landslide susceptibility assessment. Moreover, the predictive model developed in the present study is unique where only pre-earthquake landslide inventory with seismic parameter is considered to develop a hazard map to predict the landslides during future earthquakes. This is the main novelty of the work.

The landslide susceptibility index (LSI) map categorizes and quantifies the hazard-prone areas. Authorities need such maps illustrating the areas that may be affected by future landslides so that these susceptibility maps would be considered in development plans and appropriate risk mitigation measures. Such maps will be useful for planners/engineers to choose suitable localities for future development projects.

2. Study area

The study area is bounded by 30°13′48″–30°39′36″N and 79°12′36″–79°37′12″E and a part of Chamoli district of Uttarakhand state of India. The area is drained by Alaknanda River and its tributaries (figure 1). It covers the microseismic region of 1999 Chamoli earthquake (epicenter 30°24′36″N; 79°25′12″E) ranging around 1015 km^2.

The area falls under Alaknanda watershed and is characterized by different types of crystalline and lesser Himalayan rocks of the Central Crystalline Group and of Garhwal Group which are separated by a regional tectonic feature, Main Central Thrust (MCT). The region represents a tectonic terrain, characterized by thrust, local and sub-regional faults and shear zones thereby resulting in presence of low strength materials commonly associated with highly fractured rocks.

3. Spatial distribution of landslides

To perform statistical analysis on the contribution of controlling factors on the landslide activities in the study area, it is essential to identify and locate existing landslides and in this particular case to map the pre- and post-earthquake (1999 Chamoli Earthquake) landslides. In this paper, landslide inventory map is derived from Barnard *et al.* (2001). Originally Barnard *et al.* (2001) have used 338 landslides (282 pre-earthquake and 56 post-earthquake landslides). However, 276 landslides data were available to authors. This inventory is comprised of 220 pre-earthquake and 56 post-earthquake landslides. Mostly pre-earthquake landslides are rainfall induced. However, 56 post-earthquake landslides belong to Chamoli earthquake, 1999. Barnard *et al.* (2001) reported that earthquake-induced slope failures were identified by the evidence of very fresh debris on highways, trails of debris overlaying live vegetation, fresh failure scars that were free of dust and slope wash, and sometime with the help of local people. Precipitation was virtually absent from the time of the earthquake until the study was completed, insuring that most fresh slides were a direct result of the earthquake.

Details of landslide inventory are given in table 2. It is observed from the data that rock avalanche and debris avalanche type of landslides were predominantly occurred for both pre- and post-earthquake events. It has been observed that the major landslides were located on colluvium foot-slope and river terraces due to riverbank erosion. Most of these landslides occurred within 2000 m elevation as discussed later. Map of total landslide inventory is shown in figure 2. Along the NH-58 road section, some major historical landslides got reactivated often particularly during the monsoon period which disturbs the communication system and paralyze the life of the area.

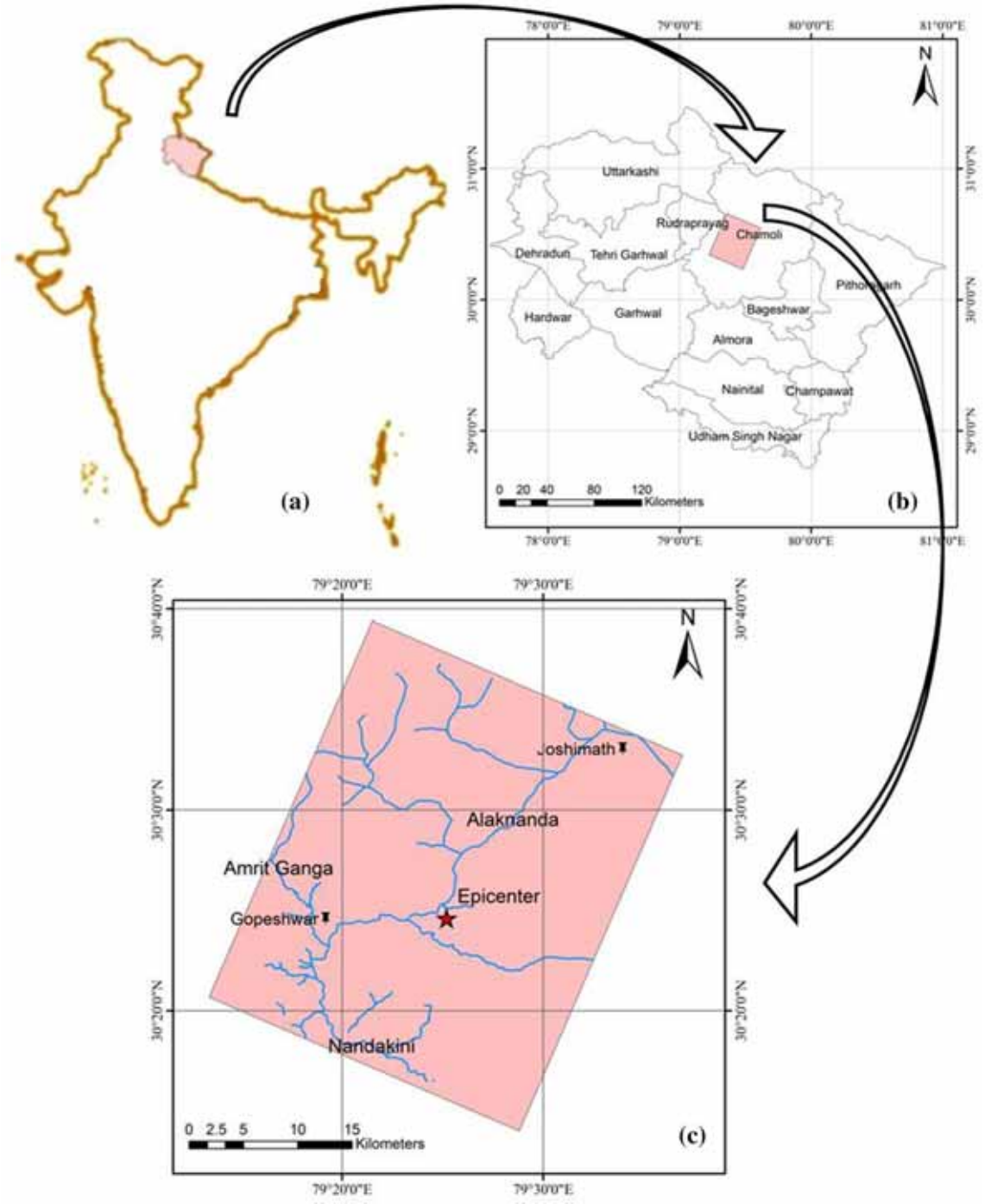

Figure 1. Location map of the study area. **(a)** Location of Uttarakhand in India, **(b)** location of Chamoli district and study area in Uttarakhand, and **(c)** location of epicenter and drainage system.

4. Analysis of landslide controlling factors

In previous studies, few controlling factors have been considered to generate landslide susceptibility zonation maps. In the present study, seven parameters are selected and these include three topographic factors (slope angle, slope aspect and slope curvature); hydrological factor (distance to drainage); geological factor (lithology); vegetation factor (normalized difference vegetation index, NDVI) and seismic factor (peak ground acceleration, PGA). Topographical and hydrological factors have been derived from CartoDEM data (July 2017) with spatial resolution of 30 m. Raster

Table 2. *Details of landslide inventory.*

	Pre-earthquake landslides (non-earthquake-induced landslides)		Post-earthquake landslides (earthquake-induced landslides)	
Type of landslides	Number	%	Number	%
Debris/rockfall	8	3.6	6	10.7
Rock avalanche	58	26.4	14	25
Debris avalanche	100	45.5	31	55.4
Debris flow	21	9.5	0	0
Debris/rock slide	33	15	5	8.9
Total	220	100	56	100

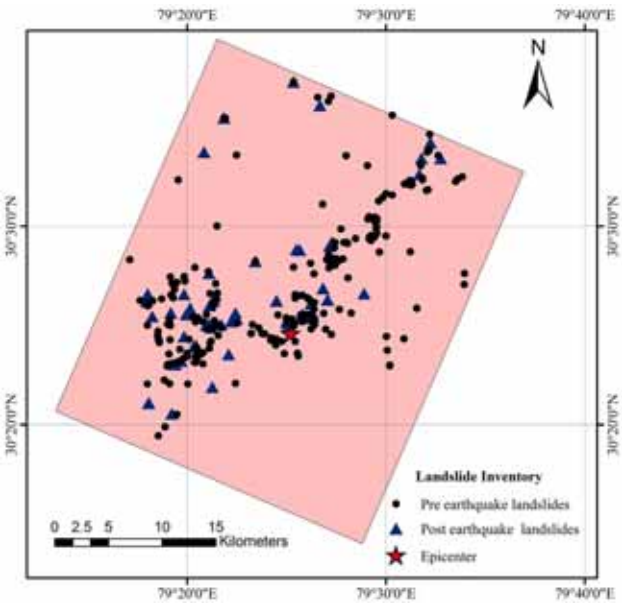

Figure 2. Landslide inventory map.

calculator tool (ArcGIS) has been used for the analysis of NDVI. Further, Landsat 8, Operational Land Imager (OLI) and Thermal Infrared Sensor (TIRS) data (July 2017) with spatial resolution of 30 m from U.S. Geological Survey (USGS) is used. Existing published map (Valdiya 1980) has been used for obtaining the lithological map. PGA map of the 1999, Chamoli earthquake as reported by Shrikhande *et al.* (2000) is used for the seismicity of the area.

It is important to report the uncertainty or error in landslide controlling factors. NRSC Report (2014) stated that the digital elevation model (DEM) effectively preserved the surface morphology, which is one of the fundamental quality considerations. The derivatives from this DEM also have shown good correspondence with the ones derived from other high resolution DEMs. NRSC Report (2014) also conducted the studies for vertical accuracy assessment that stated the Root Mean Square Error (RMSE) is in the range of 3.6–4.4 m and the LE90 is 7.2 m. In case of planimetric accuracy, the RMSE is in the range 4.5 m and CE90 is in the range 7.4–13.1 m.

Other landslide controlling factors like lineament density and rainfall are also important in LSZ mapping. It is observed that the drainage in the study area is structurally controlled in general. Hence, the lineaments are represented by the drainage lines. In the present study, distance from drainage lines (drainage buffer) is considered as one of the controlling factors. To avoid the double consideration of similar factors in terms of weightage, lineament layer is not considered as a separate controlling factor in the present study. However, the influence of lineaments is indirectly represented by the drainage layer.

Available rainfall data indicated only one data point (0.25° × 0.25° gridded rainfall data) in the study area which leads to the same distribution of rainfall for the entire study area. Therefore, the rainfall data was not considered in the present study. Present study focused on earthquake-induced susceptibility zonation so only seismic parameter, i.e., PGA has been considered in preparatory factors. Landslide controlling factor maps were produced by spatial analyst tool (ArcGIS). The following subsections provide details for the controlling factors.

4.1 *Topographic factors*

A digital elevation model (DEM) signifies the spatial variation in elevation. Figure 3(a) shows the classified DEM (30 m resolution) for the study area. In past studies also, for regional scale study 30 m resolution data was extensively used in landslide susceptibility zonation studies (Chen

et al. 2018). This DEM (figure 3a) was used to generate slope angle, slope aspect and slope curvature. It was found that the most of the landslides (88.41%) occur at lower elevation (<2000 m). Further, in the elevation range (787–1000 m) landslide density is highest.

4.1.1 *Slope angle*

Slope angle is an important controlling parameter in landslide susceptibility assessment. Slope angle is directly related to the landslide occurrence. DEM data has been used for the preparation of slope angle map. Figure 3(b) shows the slope angle map of the study area. The slope angle data is classified into six classes (<15°, 15°–25°, 25°–35°, 35°–45°, 45°–55° and >55°). Table 3 lists the landslide incidence, class area and landslide density for different factor classes. It can be observed that with the increase of slope angle, landslide incidences increase up to 35° slope angle where maximum frequency of landslide is reached. This

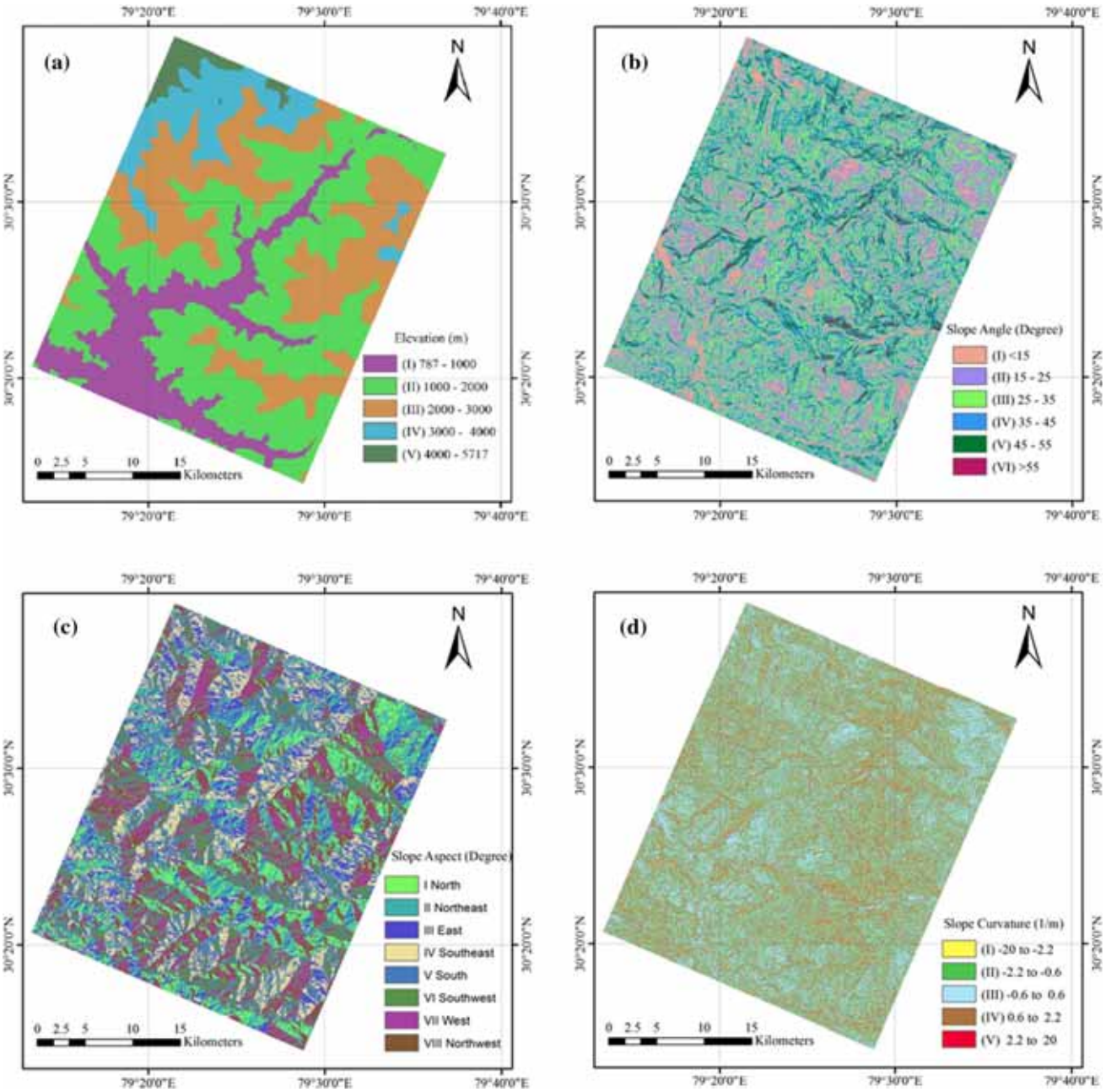

Figure 3. Topographic factors **(a)** DEM map, **(b)** slope angle map, **(c)** slope aspect map, and **(d)** slope curvature map.

Table 3. *Details of total landslide incidences, class area and landslide density with respect to factor class.*

Controlling factor	Factor class			Landslide incidence (No.) (a)	Landslide incidence (%)	Class area (km^2) (b)	Class area (%)	Landslide density (per km^2) (a/b)
Slope Angle (degree)	I	< 15	Very gentle	37	13.41	108.09	10.65	0.34
	II	15–25	Gentle	83	30.07	244.81	24.13	0.34
	III	25–35	Moderate	86	31.16	346.08	34.11	0.25
	IV	35–45	Steep	52	18.84	232.04	22.87	0.22
	V	45–55	Very steep	14	5.07	73.01	7.20	0.19
	VI	> 55	Cliff	4	1.45	10.69	1.05	0.37
Aspect (degree)	I	– 22.5 to 22.5	North	28	810.14	113.12	11.15	0.25
	II	22.5 to 67.5	Northeast	18	6.52	123.7	12.19	0.15
	III	67.5 to 112.5	East	27	9.78	124.02	12.22	0.22
	IV	112.5 to 157.5	Southeast	30	10.87	136.4	13.44	0.22
	V	157.5 to 202.5	South	49	17.75	131.42	12.95	0.37
	VI	202.5 to 247.5	Southwest	45	16.30	141.98	13.99	0.32
	VII	247.5 to 292.5	West	45	16.30	139.2	13.72	0.32
	VIII	292.5 to 337.5	Northwest	34	12.32	104.86	10.33	0.32
Profile curvature ($1/m$)	I	– 20 to – 2.2	Highly convex	9	3.26	54.95	5.42	0.16
	II	– 2.2 to – 0.6	Convex	58	21.01	241.82	23.83	0.24
	III	– 0.6 to 0.6	Flatter	131	47.46	420.45	41.44	0.31
	IV	0.6 to 2.2	Concave	62	22.46	240.02	23.65	0.26
	V	2.2 to 20	Highly concave	16	5.80	57.47	5.66	0.28
Geology	I	Saryu–Gumalikhet and Munsiari		23	8.33	358.88	35.37	0.06
	II	Granite–Granodiorite and Augen Gneiss		17	6.16	98.26	9.68	0.17
	III	Nagthat–Berinag Formations		95	34.42	136.53	13.45	0.70
	IV	Joshimath Formation		20	7.25	139.19	13.72	0.14
	V	Nathuakhan and Betalghat m. Bhatwari and Barkot units		18	6.52	16.42	1.62	1.10
	VI	Debguru Porphyroid		4	1.45	30.44	3.00	0.13
	VII	Mandhali (Sor + Thalkedar)		31	11.23	80.95	7.98	0.38
	VIII	Deoban (Gangolihat) Formation		53	19.20	133.13	13.12	0.40
	IX	Rautgara Formation		15	5.43	20.91	2.06	0.72
NDVI Index	I	– 0.1 to 0.1	Water	17	6.16	94.45	9.31	0.18
	II	0.1 to 0.2	No vegetation	61	22.10	183.98	18.13	0.33
	III	0.2 to 0.3	Very less vegetation	141	51.09	446.22	43.97	0.32
	IV	0.3 to 0.4	Less vegetation	50	18.12	263.26	25.94	0.19
	V	0.4 to 0.55	High vegetation	7	2.54	26.82	2.64	0.26
Distance to drainage (m)	I	< 500		117	42.39	222.05	21.88	0.53
	II	500 to 1000		62	22.46	202.90	20.00	0.31
	III	1000 to 1500		40	14.49	179.53	17.69	0.22
	IV	1500 to 2000		24	8.70	152.42	15.02	0.16
	V	2000 to 2500		13	4.71	110.92	10.93	0.12
	VI	> 2500		20	7.25	146.91	14.48	0.14
PGA (g)	I	0.13	High	129	46.74	163.58	16.12	0.79
	II	0.11	Moderate	82	29.71	301.52	29.71	0.27
	III	0.09	Low	55	19.93	480.22	47.33	0.11
	IV	< 0.09	Very low	10	3.62	69.38	6.84	0.14

observation is similar to that made by Dai and Lee (2002). Table 3 shows that 34.11% area is covered by moderate slope and highest landslide incidence (i.e., 31.16%). It is also observed that the gentle and moderate slope (15°–35°) classes encounter maximum of 61.23% of the total landslide incidences in the area. Topography of the study area shows that highest landslide density of 0.37 per km^2 is witnessed in cliff (>55°) class which covers only 1.05% of the total study area.

4.1.2 *Slope aspect*

Slope aspect is defined as orientation of slope. Landslide susceptibility is affected by the moisture retention and vegetation, which is related to aspect. Regmi *et al.* (2010) have shown the correlation of slope aspect with other controlling factors. The slope aspect map has been divided into eight categories namely, north, northeast, east, southeast, south, southwest, west and northwest (figure 3c). It can be observed from table 3, that south-facing slope covers 40.38% of total study area with highest landslide density of 0.37 per km^2. Less vegetation cover has been observed for south facing slopes in comparison to north facing slopes (Sinha *et al.* 1975). From this assessment, it can be concluded that south-facing slopes are more susceptible to landslides.

4.1.3 *Slope curvature*

Slope curvature is the second derivative of DEM. Profile curvature has been considered in the present study. Positive values denote the upwardly concave and negative values denote upwardly convex terrain. Zero values denote the flat terrain. Curvature map has been produced from DEM and classified in five categories: Highly convex (–20 to –2.2), convex (–2.2 to –0.6), flatter (–0.6 to 0.6), concave (0.6 to 2.2) and highly concave (2.2–20). Slope curvature map of the study area is given in figure 3(d). Statistics related to distribution of landslides in curvature classes are shown in table 3. It shows that landslide density is more in highly concave, concave and flatter class that occupies 71% of the total study area. These concave hill slopes are having high soil moisture content and receive more surface run-off. So, it can be stated that concave and flatter slopes are more susceptible than convex slopes.

4.2 *Geological factor: Lithology*

Spatial distribution of various lithological units is presented in figure 4(a). Details of each factor class (I to IX) are given in table 3. Geologically, the rocks of the study area can be categorized into six lithological units, viz., Almora Group, Jaunsar Group, Vaikrita Group, Ramgarh Group, Tejam Group and Damtha Group. Present study area consists of different rocks like gneiss, phyllites, granite to granodiorite, slate, dolomite and limestone. As shown in table 3, highest landslide density of 1.10 per km^2 is obtained for Nathuakhan and Betalghat, Bhatwari and Barkot Formation followed by that of 0.72 per km^2 for Rautgara Formation. The study area consists of various faults, folds and thrusts and has undergone severe weathering and erosion by river network, which has increased the susceptibility of landslides in the rock units.

Lithological information has been derived from the existing geological map of the study area (Valdiya 1980). Rocks having some inherent property like compactness, composition and structure, which show different resistance against erosion and weathering. Soft rocks like slates and phyllites are more prone to landslides than compact and hard rocks like limestone and granite.

4.3 *Vegetation index: NDVI*

NDVI value represents the variation of vegetation in the area. High NDVI values represent healthy vegetation and negative values represent the bare areas and water bodies. NDVI map (before and after 1999 Chamoli earthquake) has been reported by Sangeeta and Maheshwari (2018) and it was concluded that NDVI is an important controlling factor. NDVI map (figure 4b) was developed from LANDSAT 8 Operational Land Imager (OLI) and Thermal Infrared Sensor (TIRS) imagery using Band 4 and 5. Table 3 indicates that very less vegetation region (0.2–0.3) contains 51% of landslide incidences (141 landslides) and a landslide density of 0.32 per km^2 is obtained.

4.4 *Hydrological factor: Distance to drainage*

Natural drainages initiate landslides either by cutting the toe of a slope or by eroding downstream along the slope. Therefore, drainage to distance has

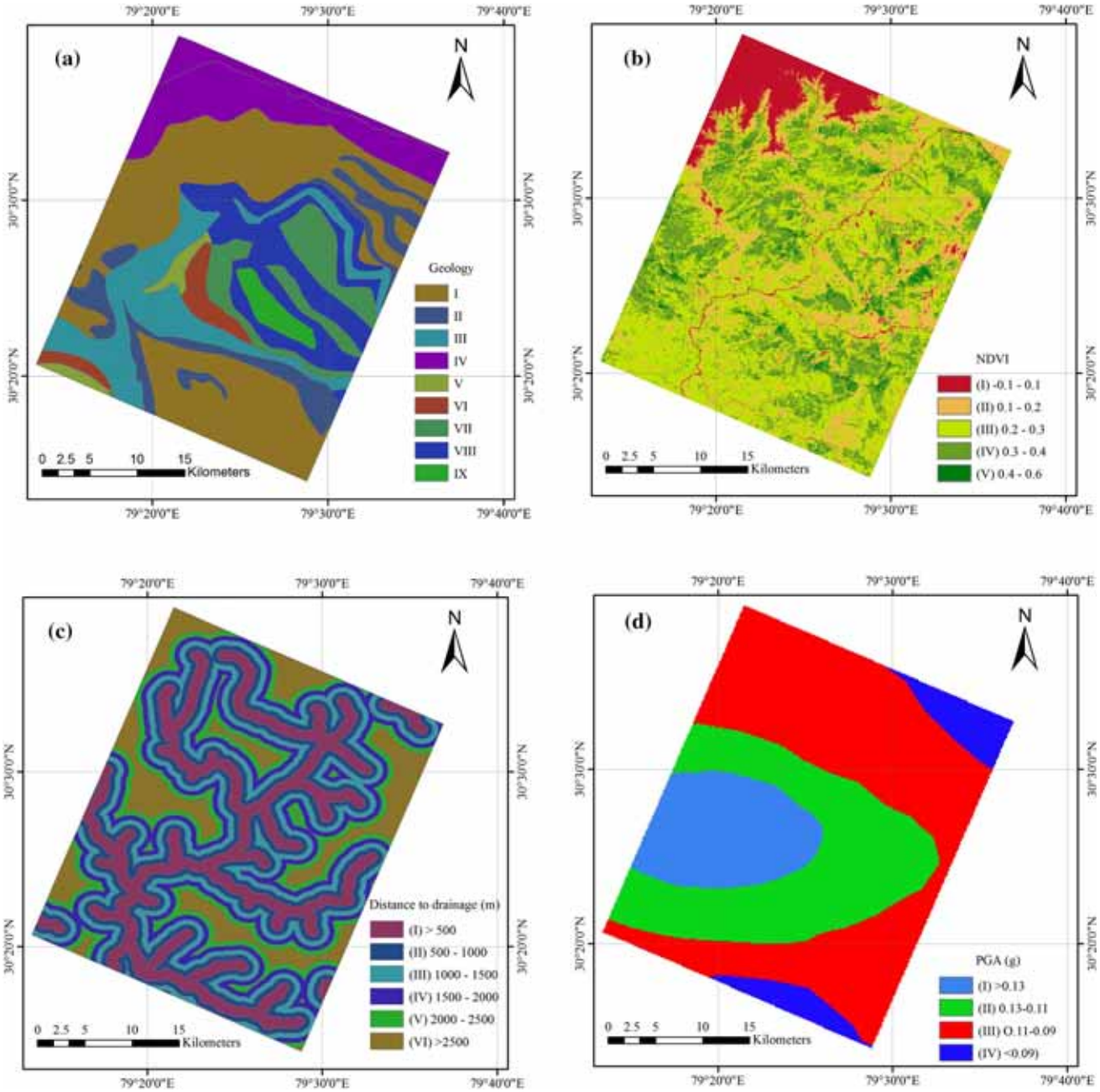

Figure 4. **(a)** Geological map, **(b)** NDVI map, and **(c)** distance to drainage map, and **(d)** PGA map.

also been adopted as a main causative parameter. In this study, a drainage map with different orders of streams was extracted from 30 m DEM using hydrology tool of Arc GIS. As it was observed that in the study area lower order drainages contribute significantly to landslide activities, drainages up to 3rd order was considered for the analysis and multiple ring buffers were created around them to the extent that the entire study area is covered. For the purpose of analysis, buffer map with 500 m distance intervals to drainage has been prepared and classified into six categories i.e., <500, 500–1000, 1000–1500, 1500–2000, 2000–2500 and >2500. Drainage buffer map is shown in figure 4(c).

Flow rate and lithology of the area are the main reasons for the river erosion and weathering process. It was witnessed that the density of landslides is more in the near vicinity of drainages that are more prone for weathering and erosion. Table 3 shows that 42.39% of landslides are falling in <500 m drainage buffer zone with highest landslide density of 0.53 per km^2. The landslide density

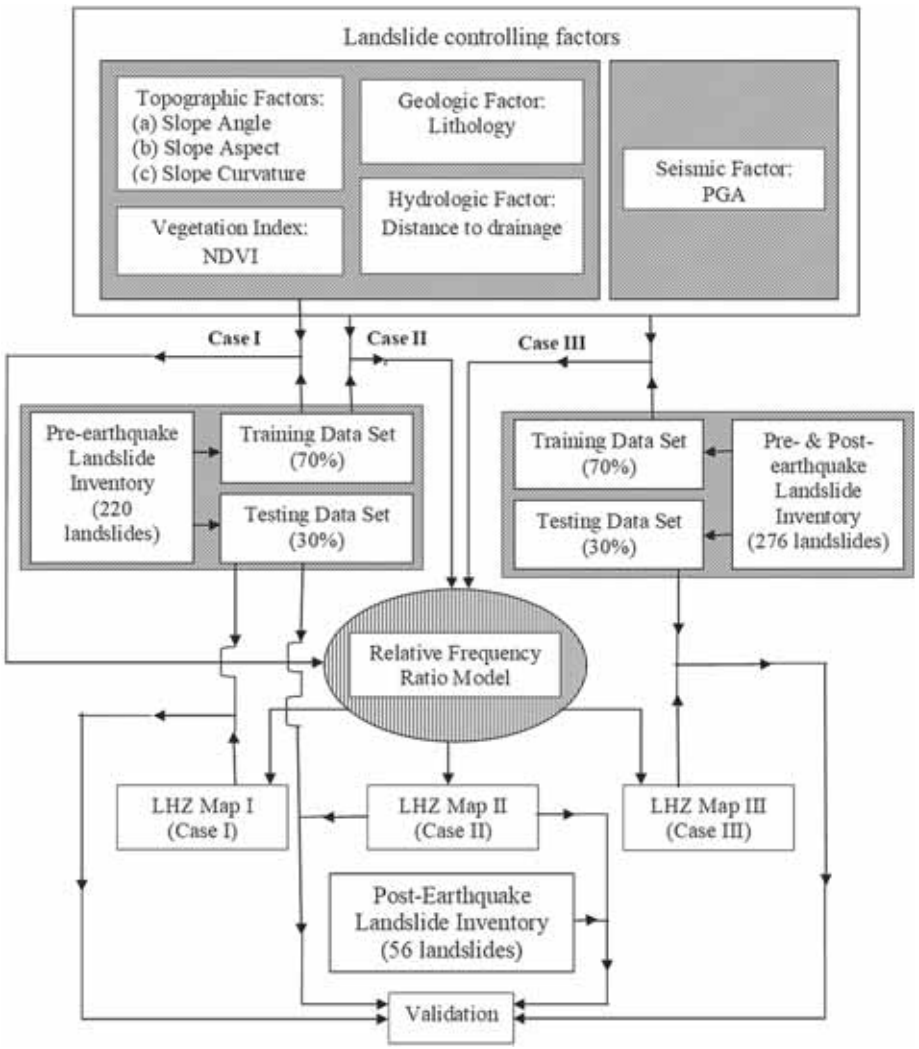

Figure 5. Flowchart of working methodology.

value decreases as the distance from the drainage lines increases.

4.5 *Seismic factor: PGA*

In 1999, Chamoli district witnessed an earthquake of magnitude (M_s 6.6) that induced 56 landslides in the study area. PGA can be taken as a controlling parameter to examine the landslide susceptibility (Wang *et al.* 2011). Present study used a four PGA contour zones (i.e., >0.13, 0.11–0.13, 0.09–0.11 and <0.09 g) corresponding to 1999 Chamoli earthquake. Figure 4(d) presents the PGA map of the study area, derived from Shrikhande *et al.* (2000). Statistics given in table 3 indicate that highest landslide density of 0.79 per km^2 is observed in >0.13 g contour zone. This is near the epicenter where tear faults and Main Central Thrust (MCT) intersects.

5. Methodology

The processes involved in the present work include input data preparation and its processing, pre- and post-earthquake landslide susceptibility zonation map generation and evaluation of the effect of seismic parameter on landslide susceptibility assessment. In this study, landslide susceptibility zonation mapping in the considered region has been carried out using relative frequency ratio (RFR) model. RFR is similar to the relative landslide density index (Baeza and Corominas 2001) and frequency ratio (FR) model (Lee and Min 2001).

Frequency ratio (FR) gives proportion of the landslide occurrences in a particular class for each of the controlling factors. It is calculated as a ratio of landslide incidence (%) in factor class to the area (%) of that factor class. This method follows the

Table 4. *Frequency ratio (FR) and relative frequency ratio (RFR) of the landslide controlling factor classes for preparation of LSZ maps (Case I, II and III).*

			Case (I and II) pre-earthquake				Case (III) post-earthquake			
Controlling factor	Factor class*	Class area (%)	Landslide incidence (No.)	Landslide incidence (%)	FR	RFR	Landslide incidence (No.)	Landslide incidence (%)	FR	RFR
Slope angle (degree)	I	10.65	15	9.62	0.903	0.137	23	11.73	1.102	0.163
	II	24.13	50	32.05	1.328	0.202	61	31.12	1.290	0.191
	III	34.11	53	33.97	0.996	0.151	63	32.14	0.942	0.139
	IV	22.87	26	16.67	0.729	0.111	35	17.86	0.781	0.115
	V	7.19	9	5.77	0.802	0.122	10	5.10	0.709	0.105
	VI	1.05	3	1.92	1.826	0.277	4	2.04	1.937	0.287
Aspect (degree)	I	11.15	18	11.54	1.035	0.148	22	11.22	1.007	0.112
	II	12.19	7	4.49	0.368	0.040	11	5.61	0.460	0.051
	III	12.22	15	9.62	0.787	0.086	16	8.16	0.668	0.073
	IV	13.44	12	7.69	0.572	0.063	16	8.16	0.607	0.067
	V	12.95	30	19.23	1.485	0.163	37	18.88	1.458	0.160
	VI	13.99	25	16.03	1.145	0.126	32	16.33	1.167	0.128
	VII	13.72	29	18.59	1.355	0.149	35	17.86	1.302	0.143
	VIII	10.33	20	12.82	1.241	0.136	27	13.78	1.333	0.147
Profile curvature ($1/m$)	I	5.42	4	2.56	0.473	0.107	7	3.57	0.659	0.144
	II	23.83	30	19.23	0.807	0.183	40	20.41	0.856	0.187
	III	41.44	74	47.44	1.145	0.259	91	46.43	1.121	0.245
	IV	23.65	40	25.64	1.084	0.246	48	24.49	1.035	0.226
	V	5.66	8	5.13	0.905	0.205	10	5.10	0.901	0.197
Geology	I	35.37	19	12.18	0.344	0.026	21	10.71	0.303	0.022
	II	9.68	9	5.77	0.596	0.044	13	6.63	0.685	0.05
	III	13.45	48	30.77	2.287	0.17	66	33.67	2.503	0.182
	IV	13.71	13	8.33	1.099	0.081	15	7.65	0.968	0.07
	V	1.62	9	5.77	3.566	0.265	11	5.61	3.469	0.253
	VI	3	1	0.64	0.214	0.016	3	1.53	0.51	0.037
	VII	7.98	23	14.74	1.848	0.138	24	12.24	1.535	0.112
	VIII	13.12	27	17.31	1.319	0.098	33	16.84	1.283	0.093
	IX	2.07	7	4.49	2.177	0.162	10	5.1	2.476	0.18
NDVI index	I	9.31	12	7.69	0.826	0.180	12	6.12	0.658	0.144
	II	18.13	33	21.15	1.167	0.254	46	23.47	1.294	0.283
	III	43.97	78	50.00	1.137	0.247	97	49.49	1.125	0.246
	IV	25.94	30	19.23	0.741	0.161	37	18.88	0.728	0.159
	V	2.64	3	1.92	0.728	0.158	4	2.04	0.772	0.169
Distance to drainage (m)	I	21.88	68	43.59	1.992	0.375	84	42.86	2.143	0.387
	II	20.00	40	25.64	1.282	0.241	49	25.00	1.413	0.255
	III	17.69	18	11.54	0.652	0.123	24	12.24	0.815	0.147
	IV	15.02	14	8.97	0.597	0.112	16	8.16	0.747	0.135
	V	10.93	6	3.85	0.352	0.066	10	5.10	0.352	0.064
	VI	14.48	10	6.41	0.443	0.083	13	6.63	0.066	0.012
PGA (g)	I	16.12	59	37.82	2.346	0.494	86	43.88	2.722	0.576
	II	29.71	46	29.49	0.992	0.209	58	29.59	0.996	0.211
	III	47.33	42	26.92	0.569	0.120	45	22.96	0.485	0.103
	IV	6.84	9	5.77	0.844	0.178	7	3.57	0.522	0.111

*Refer table 3 for factor class details.

theory of conditional probability for which the ratio >1 displays a high probability of landslide occurrence and the ratio <1 represents low probability. Higher is the frequency ratio number for a factor class, higher is the influence of that particular class on the landslide occurrence.

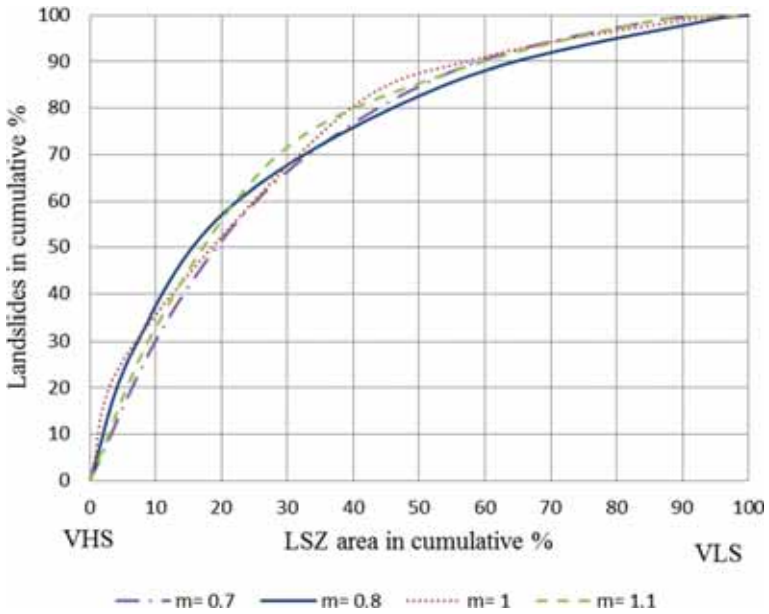

Figure 6. Success rate curves for different m values (Case I).

Frequency ratio (FR) and relative frequency ratio (RFR) have been used to correlate landslide inventory and controlling parameters, where equations (1 and 2) are used for the calculation of FR and RFR respectively.

$$FR_{i,j} = \frac{N_{i,j}/\sum N_{i,j}}{A_{i,j}/\sum A_{i,j}}, \tag{1}$$

where $FR_{i,j}$ represents frequency ratio of ith class of jth factor. $N_{i,j}$ is defined as number of landslides in ith class of jth factor and $A_{i,j}$ is area of ith class of jth factor.

$$RFR_{i,j} = \frac{FR_{i,j}}{\sum FR_{i,j}}. \tag{2}$$

Firstly, $RFR_{i,j}$ values are assigned to each factor class after multiplying them by 100. Then the RFR maps of all the factors were combined linearly in order to get the LSI map.

All this analysis has been performed in GIS on a raster format with pixel size of 30 m×30 m. Total study area of 1014.72 km^2 accounts for 1.127×10^6 number of pixels. The LSI is calculated by equation (3):

$$\text{LSI} = \sum_{i=1,j=1}^{n,m} RFR_{i,j}, \tag{3}$$

where n is the number of classes and m is the number of factors. LSI values were divided into five classes based on different hazard levels, as explained in section 6. Firstly, LSZ map of the study area was prepared by pre-earthquake landslide inventory and assessed the effect of the seismic parameter. Then, earthquake-induced LSZ map was generated by landslide inventory, which also included earthquake-induced landslide inventory. Flowchart to detremine LSZ map and its validation is given in figure 5 for three cases, i.e., Case I, II and III defined as follows:

Case I: considering pre-earthquake landslide inventory without seismic factor.

Case II: considering pre-earthquake landslide inventory with seismic factor.

Case III: considering pre- and post-earthquake-landslide inventory with seismic factor.

6. Landslide susceptibility assessment using RFR model

To perform RFR analysis, all the factor maps are analysed spatially with respect to the landslide inventory map in classified raster format using ArcGIS. Based on the spatial analysis, the FR and RFR values for all the factor classes have been calculated for different cases of LSZ maps (I, II and III). Based on the RFR and LSI maps have been generated. Depending on the LSI values, the whole study area has been divided into five different classes of landslide susceptibility as very low susceptibility (VLS), low susceptibility (LS), medium

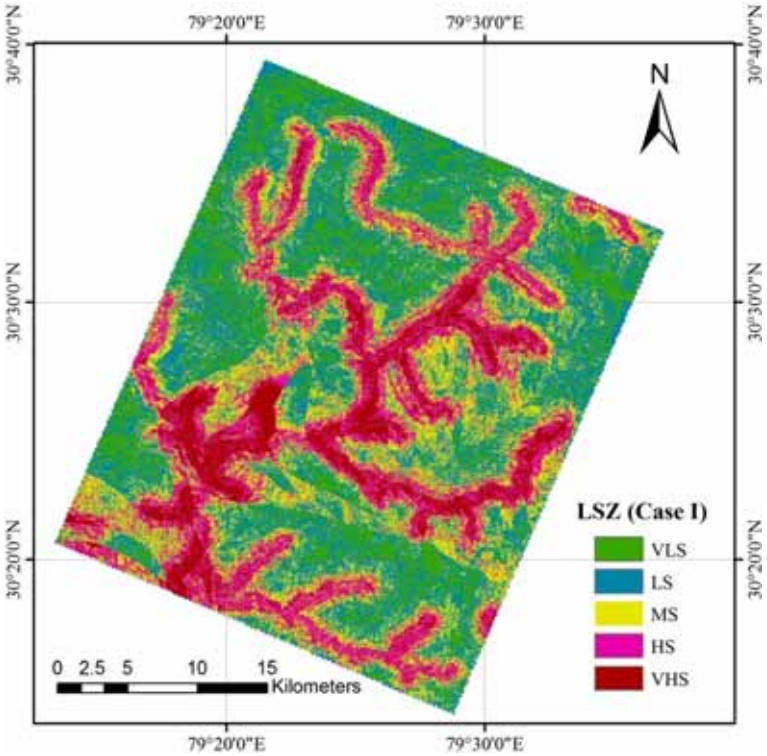

Figure 7. LSZ map for Case I.

Table 5. *Classification of different susceptibility class for Case I.*

Susceptibility class	LSI range	Area (km^2)	Area (%)	Landslide incidence training (No.)	Landslide incidence training (%)	Landslide incidence testing (No.)	Landslide incidence testing (%)
VLS	52–81	159.95	15.76	7	4.49	1	1.56
LS	81–94	304.22	29.98	18	11.54	7	10.94
MS	94–107	257.59	25.39	33	21.15	11	17.19
HS	107–120	186.05	18.34	44	28.21	23	35.94
VHS	120–159	106.91	10.54	54	34.62	22	34.38

susceptibility (MS), high susceptibility (HS) and very high susceptibility (VHS).

6.1 *Case I: LSZ map using pre-earthquake landslide inventory without seismic factor*

To prepare this LSZ map, six controlling factors, i.e., slope angle, slope aspect, slope curvature, distance to drainage, NDVI and geology have been used. The seismic factor (PGA) has not been considered in this case. Pre-earthquake landslide inventory of 220 landslides is divided into training and testing datasets. Training dataset having about 70% of the total database (i.e., 156 landslides) was used to build the model and produce LSZ map. Testing dataset having 30% of the total landslides (i.e., 64 landslides) used for the validation of the model and thereby the LSZ map. The computation of FR and RFR for various factor classes is presented in table 4. For Case I, last row of this table, i.e., PGA is not used while for Case II, all rows are used.

For the classification of LSI boundaries, a method proposed by Saha *et al.* (2005) is adopted, which is a statistical based method that reduces the subjectivity.

Range of LSI values obtained in Case I was from 52 to 159. The mean (μ) and standard deviation (σ) calculated by best-fit probability distribution curve are 100.56 and 16.125, respectively. LSI values were classified into five susceptibility classes with boundaries at ($\mu - 1.5\,m\sigma$), ($\mu - 0.5\,m\sigma$), ($\mu + 0.5\,m\sigma$) and

($\mu + 1.5\, m\sigma$). Here m is a number greater than zero (Saha *et al.* 2005; Kanungo *et al.* 2006). The m value governs the most suitable boundaries within the LSI range. LSZ maps have been produced for four m values (0.7, 0.8, 1.0 and 1.1).

The cumulative percentages of landslide incidences in all five susceptibility class were plotted against the cumulative percentage of the area of the susceptibility class for these LSZ maps. Chung and Fabbri (1999) defined the success rate curves which used to select the suitable values of m to decide the appropriateness of an LSZ map. Figure 6 shows success rate curves for different m values. LSZ map which contains more landslides in VHS class will be considered most suitable.

It can be observed from figure 6 that for 10% of the area in VHS class, the curves corresponding to $m = 0.7$, 0.8, 1.0 and 1.1 show the landslide occurrences of 30%, 34%, 32%, and 31%, respectively. This shows that first 10% area, the curve corresponding to m 0.8 has the highest success rate, i.e., 34%. So, m at 0.8 appears to be the most appropriate one for the study area. Accordingly, the landslide susceptibility class boundaries were classified at LSI values of 81, 94, 107 and 120. The LSZ map (Case I) thus produced is shown in figure 7.

Table 5 shows the details of different susceptibility class. It can be observed that 55.37% of the study area is falling under LS and MS classes. VHS class is covering only 10.54% of the study area but the majority of landslide incidence, i.e., 34% is falling in this class. Major parts of Chamoli town falls under VHS and HS class. Further, most part of the Joshimath (subdistrict) are falling in MS LS and VLS class and the area which lies in the lower altitude falls under HS and VHS class. This model has been validated by testing dataset. Table 5 also shows the validation result. All the susceptibility classes are in good agreement with the model results.

6.2 *Case II: LSZ map using pre-earthquake landslide inventory with seismic factor*

1999 Chamoli earthquake induced 56 landslides in the study area and also reactivated the old landslides. Therefore, the seismic parameter is important and has been included along with various other factors while carrying out landslide susceptibility assessment.

To prepare this LSZ map, six controlling factors including slope angle, slope aspect, slope curvature, distance to drainage, NDVI and geology along with the seismic parameter (PGA) have been used. Pre-earthquake landslide inventory of 220 landslides is divided into two datasets: a training dataset having 70% of the total database (i.e., 156 landslides) which was used to build the model and produce LSZ map; and a testing dataset having 30% of the total landslides (i.e., 64 landslides) used for the validation of the model and thereby the LSZ map. Also, the post-earthquake landslide inventory of 56 earthquake-induced landslides was also used for the model validation and thereby the LSZ map.

In this case, the LSI values were ranging between 64 and 209. Similar to Case I, mean and standard deviation are obtained as 122.79 and 22.362, respectively, and success rate curves were calculated for $m = 0.7$, 0.8, 1 and 1.1. The curves (figure 8) corresponding to $m = 0.7$, 0.8, 1.0 and 1.1 show the landslide occurrences of 33%, 38%, 34% and 32%, respectively. LSZ map at $m = 0.8$ appears to be the most appropriate due to highest success rate value. On the basis of analysis, the landslide susceptibility class boundaries were fixed at LSI values of 96, 114, 132 and 150. The LSZ map (Case II) thus produced is shown in figure 9. Table 6 represents the details of different landslide susceptibility class in terms of area and landslide incidence. LSZ map indicates that after including seismic parameter, VHS class clustered around the epicenter of 1999 Chamoli earthquake.

It can be perceived from table 6 that after including seismic factor, VHS class in the LSZ map (Case II) has occupied 9.04% of the total study area. If these results are compared with LSZ map (Case I), cumulative area of VLS, LS and MS classes has increased while that of HS and VHS classes has decreased. Also VHS class is clustered near epicenter. Therefore, it can be stated that there is a significant effect of seismic factor over this LSZ map.

In the absence of earthquake induced landslide inventory, LSZ map (Case II) can be used as earthquake induced landslide predictive model. This model is also validated with earthquake-induced landslide inventory (56 landslides). Table 6 shows that maximum and minimum landslides are falling in VHS and VLS class. Hence, the model is also well validated against earthquake-induced landslides. Therefore, it may be stated that inclusion of seismic factor in generation of LSZ map can also spatially predict the earthquake-induced landslides in a better way.

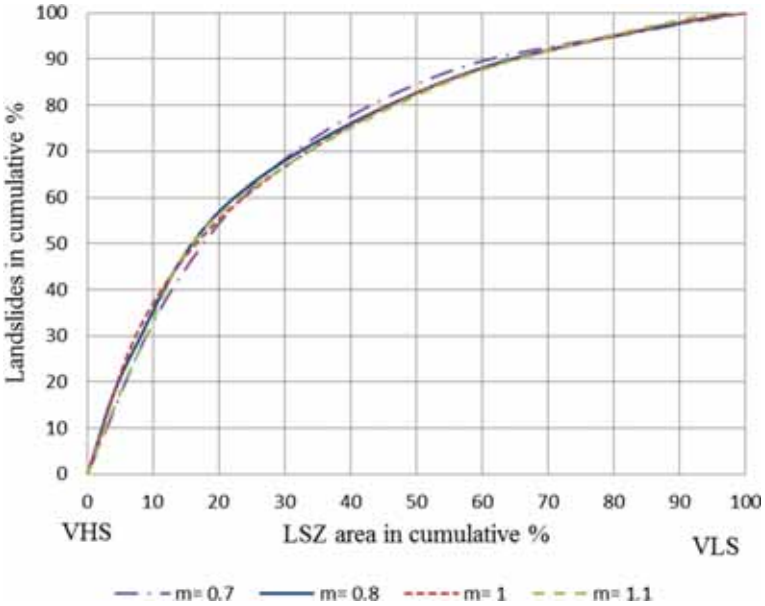

Figure 8. Success rate curves for different m values (Case II).

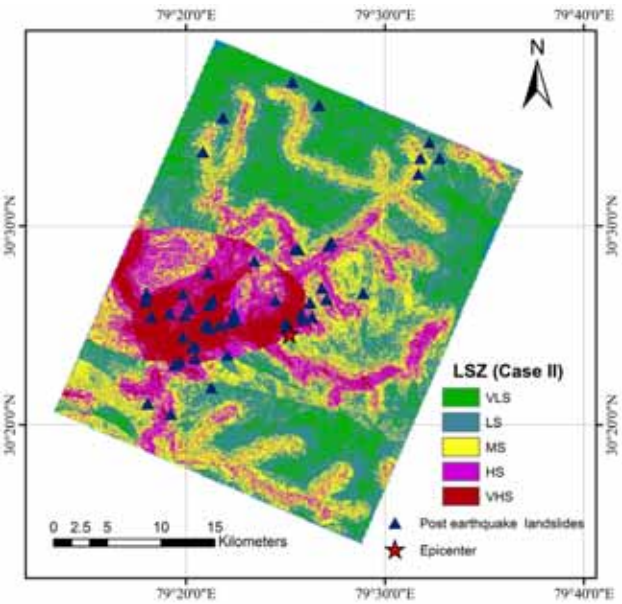

Figure 9. LSZ map for Case II.

6.3 *Case III: LSZ map using pre- and post-earthquake landslide inventory with seismic factor*

Earthquake-induced landslides due to 1999 Chamoli earthquake has been reported in many articles (Rajendran *et al.* 2000; Barnard *et al.* 2001). In the present work, 1999 Chamoli earthquake has been selected as a scenario earthquake. For this purpose, the landslide inventory with pre- and post-earthquake landslides with a total of 276 landslides (training: 196 and testing: 80) is used.

Table 4 shows the frequency ratio (FR) and relative frequency ratio (RFR) calculation of the landslide controlling factor for post-earthquake scenario. For the preparation of this LSZ map, the same controlling factors have been used as in Case II. However, in this case, the contribution of each controlling factor has been found to be changed, as compared to previous two cases, perhaps due to change in landslide inventory, i.e., an earthquake phenomenon changes the landslide incidence.

The LSI values were falling in the range between 67 and 222. The mean (μ) and standard deviation (σ) calculated from best-fit probability distribution curve are 128.43 and 24.62, respectively. Figure 10 shows the success rate curves for $m = 0.7$, 0.8, 1 and 1. It has been noted that for 10% area of VHS class, the curves respective to $m = 0.7$, 0.8, 1.0 and 1.1 show the landslide occurrences of 32%, 42%, 40% and 39%, respectively. This analysis shows that m at 0.8 gives most appropriate LSZ map for the study area. Therefore, the landslide susceptibility were classified at LSI values of 99, 119, 138 and 158. The LSZ map (Case III) thus produced is shown in figure 11. Table 7 represents the area covered by different susceptibility classes along with landslide incidences.

It can be observed from table 7 that after including the earthquake-induced landslides in the

Table 6. *Classification of different susceptibility class for Case II.*

Susceptibility class	LSI range	Area (km^2)	Area (%)	Landslide incidence training (No.)	Landslide incidence training (%)	Landslide incidence testing (No.)	Landslide incidence testing (%)	Earthquake induced landslide (No.)	Earthquake induced landslide (%)
VLS	64–96	166.05	16.36	6	3.85	2	3.13	3	5.36
LS	96–114	319.93	31.53	19	12.18	3	4.69	5	8.93
MS	114–132	279.77	27.57	36	23.08	17	26.56	8	14.29
HS	132–150	157.25	15.50	41	26.28	14	21.88	15	26.79
VHS	150–209	91.72	9.04	54	34.62	28	43.75	25	44.64

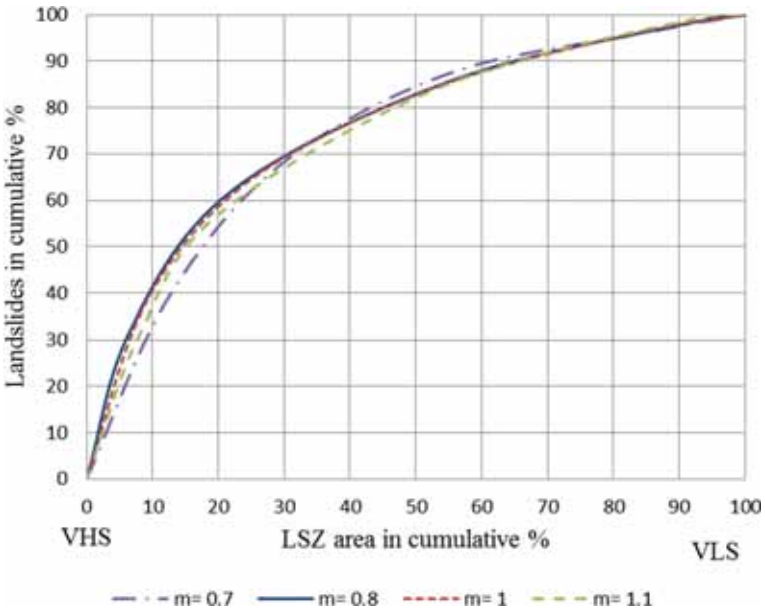

Figure 10. Success rate curves for different m values (Case III).

inventory database, the VHS class in the LSZ map (Case III) has occupied 10.06% of the total study area. If these results are compared with previous LSZ maps (Case I and II), cumulative area of VLS, LS and MS classes and that of HS and VHS classes in this case (Case III) lie within the values of both the previous cases. Table 7 also indicates that 42% of the landslides from the training dataset fall within the VHS class. It can be observed that VHS class has increased near epicenter in LSZ map. This is due to the fact that earthquake-induced landslides are clustered near the epicenter.

6.4 *Comparative evaluation and error estimation of LSZ maps*

The comparison of all three LSZ maps has been carried out based on the distribution of landslide densities in different susceptibility zones for both training and testing landslide data as previously discussed in sections 6.1–6.3. The landslide densities for training datasets are given in table 8 and those for testing datasets are given in table 9.

Table 8 shows that all the LSZ maps for three different cases have displayed reasonably very good success rate accuracies in terms of landslide densities (lowest in case of VLS, highest in case of VHS and following an increasing trend from VLS to VHS with a minor exception in case of LSZ Map III where LS has a marginally less landslide density in comparison to that of VLS) for the training datasets based on which these models are built. These results show that the success rates of all these models are high as usually expected. It is further observed that the LSZ Maps II and III are better

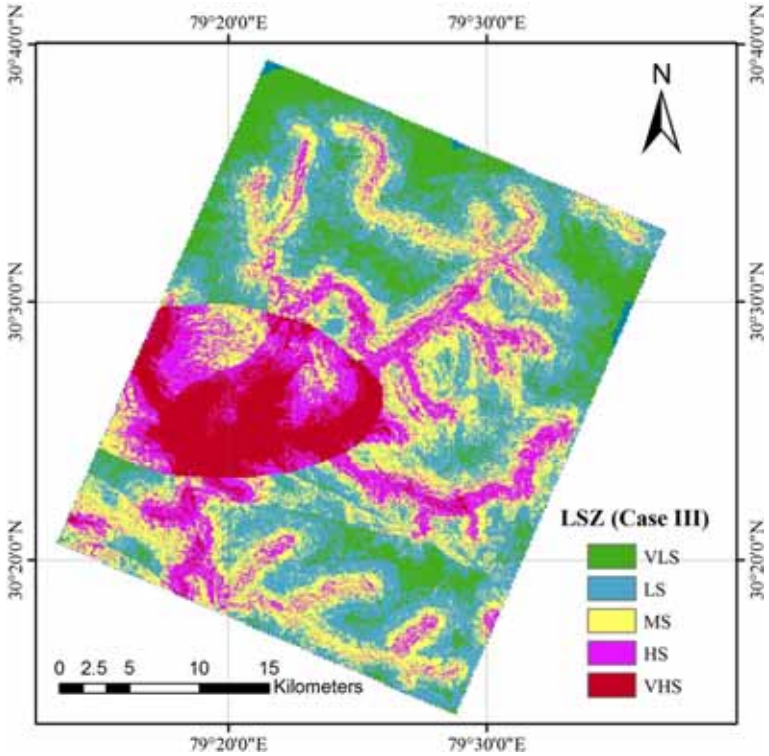

Figure 11. LSZ map for Case III.

Table 7. *Classification of different susceptibility class for Case III.*

Susceptibility class	LSI range	Area (km^2)	Area (%)	Landslide incidence training (No.)	Landslide incidence training (%)	Landslide incidence testing (No.)	Landslide incidence testing (%)
VLS	67–99	144.64	14.25	8	4.08	1	1.25
LS	99–119	317.43	31.28	15	7.65	7	8.75
MS	119–138	283.83	27.97	38	19.39	15	18.75
HS	138–158	166.71	16.43	52	26.53	20	25.00
VHS	158–222	102.1	10.06	83	42.35	37	46.25

Table 8. *Distribution of landslide densities in different LSZ maps for training datasets.*

	LSZ (Case I)			LSZ (Case II)			LSZ (Case III)		
LSZ class	Area (%) (a_1)	Landslide incidence (%) (b_{tr1})	Density (b_{tr1}/a_1)	Area (%) (a_2)	Landslide incidence (%) (b_{tr2})	Density (b_{tr2}/a_2)	Area (%) (a_3)	Landslide incidence (%) (b_{tr3})	Density (b_{tr3}/a_3)
VLS	15.76	4.49	0.285	16.36	3.85	0.235	14.25	4.08	0.286
LS	29.98	11.54	0.385	31.53	12.18	0.386	31.28	7.65	0.244
MS	25.39	21.15	0.833	27.57	23.08	0.837	27.97	19.39	0.693
HS	18.34	28.21	1.538	15.5	26.28	1.695	16.43	26.53	1.615
VHS	10.54	34.62	3.285	9.04	34.62	3.830	10.06	42.35	4.209

with higher success rate accuracies in terms of reasonably higher landslide densities for HS and VHS zones as compared to those of LSZ Map I.

Similarly, it is observed from table 9 that all the LSZ maps for three different cases have displayed reasonably very good validation accuracies in

Table 9. *Distribution of landslide densities in different LSZ maps for testing datasets.*

	LSZ (Case I)			LSZ (Case II)					LSZ (Case III)		
	Pre-earthquake landslides			Pre-earthquake landslides			Post-earthquake landslides		Pre-earthquake landslides		
LSZ class	Area (%) (a_1)	Landslide incidence (%) (b_{ts1})	Density (b_{ts1}/a_1)	Area (%) (a_2)	Landslide incidence (%) (b_{ts2})	Density (b_{ts2}/a_2)	Landslide incidence (%) (b_{tsp2})	Density (b_{tsp2}/a_2)	Area (%) (a_3)	Landslide incidence (%) (b_{ts3})	Density (b_{ts3}/a_3)
VLS	15.76	1.56	0.099	16.36	3.13	0.191	5.36	0.328	14.25	1.25	0.088
LS	29.98	10.94	0.365	31.53	4.69	0.149	8.93	0.283	31.28	8.75	0.280
MS	25.39	17.19	0.677	27.57	26.56	0.963	14.29	0.518	27.97	18.75	0.670
HS	18.34	35.94	1.960	15.5	21.88	1.412	26.79	1.728	16.43	25.00	1.522
VHS	10.54	34.38	3.262	9.04	43.75	4.840	44.64	4.938	10.06	46.25	4.597

terms of landslide densities (lowest in case of VLS, highest in case of VHS and following an increasing trend from VLS to VHS with a minor exception in case of LSZ Map II where LS has a marginally less landslide density in comparison to that of VLS for both pre- and post-earthquake testing datasets) for the testing datasets based on which the developed models and LSZ maps are validated. It is further observed that the LSZ Maps II is better with higher validation accuracy in terms of reasonably higher landslide densities for VHS zones for both pre- and post-earthquake landslide testing datasets as compared to those of LSZ Map I and III.

The Case II model and subsequently the LSZ Map II is developed based on the controlling factors including seismic parameter and pre-earthquake landslide inventory excluding the earthquake-induced (post-earthquake) landslides and could predict both pre- and post-earthquake landslides as observed in validation results through testing datasets. Therefore, it can be concluded in a sense that the Case II model of LSZ map preparation is the ideal one with overall very good success rate and validation accuracies for spatial prediction of both pre- and post-earthquake landslide zones.

Also from tables 8 and 9, it can be observed that for all three cases, the maximum percentage landslides occur in VHS class even though % area is the minimum for this class.

Researchers have used different methods such as area under curve (AUC), receiver operating characteristics (ROC), mean square error (MSE) and root mean square error (RMSE) to evaluate the performance of models (Chen *et al.* 2018; Nguyen *et al.* 2019). In this study, root mean square error (RMSE) was used to validate the performance of the developed models. The RMSE measures the forecasting errors of the models (Gorum *et al.* 2008). The RMSE can be expressed as follows:

$$\mathrm{RMSE} = \sqrt{\frac{1}{n}\sum\left(X_{\mathrm{predicted}} - X_{\mathrm{observed}}\right)^2}, \qquad (4)$$

where n is total sample in the dataset, $X_{\mathrm{predicted}}$ is the predicted values in the training dataset and X_{observed} is the testing values from the dataset. In terms of the RMSE, Case III had the lowest value (0.023), followed by Case I (0.041) and Case II (0.058). The results confirmed that all three cases have reasonable accuracy (RMSE $< 6\%$) for LSZ mapping, and Case III had the best accuracy.

7. Conclusions

In the present work, relative frequency ratio (RFR) method is adopted to develop the landslide susceptibility zonation (LSZ) maps with three different combinations of controlling factors and landslide inventories in GIS platform for part of Chamoli district, Uttarakhand, India. The LSZ map spatially predicts the potential landslide susceptible areas in terms of severity of the hazard class. In the LSZ maps, whole area is classified in five groups, i.e., very low susceptibility (VLS), low susceptibility (LS), medium susceptibility (MS), high susceptibility (HS) and very high susceptibility (VHS). The study highlights the need of including the seismic parameter accompanied by other static factors for LSZ mapping in an earthquake-prone area like Himalayas. Major conclusions and findings drawn from the present study are as follows:

- Three LSZ maps, two using pre-earthquake landslide inventory (maps I and II) and one using both pre and post-earthquake landslide

inventory (map III) were developed. The results show that the LSZ Maps II and III are better with higher success rate accuracies in terms of reasonably higher landslide densities for HS and VHS zones as compared to those of LSZ Map I.

- Further, it can be concluded that the Case II model of LSZ map preparation is the ideal one with overall very good success rate and validation accuracies for spatial prediction of both pre- and post-earthquake landslide zones.
- In the absence of earthquake-induced landslide inventory, LSZ map (Case II) can be used as earthquake-induced landslide predictive model.
- Majority of the study area that falls into VHS class is concentrated around Chamoli town, which is a base camp for the tourist activities.

The presented research work has much practical significance. This is because of high possibility of devastating earthquake exists in Uttarakhand due to high seismicity. Landslide susceptibility zonation maps, which include earthquake-induced inventory and seismic parameter, are helpful for the state government and disaster mitigation and management agencies to take necessary action against any up-coming seismic activity. Hence, this research can be helpful for the planners/designers and engineers to select suitable area for the development projects.

Acknowledgement

The fellowship to the first author from Ministry of Human Resource Development (MHRD), Govt. of India, for this research work is gratefully acknowledged.

References

Abou-Jaoude G, Saade A, Wartman J and Grant A 2016 Earthquake-induced landslide hazard mapping: A case study in Lebanon; Geo-Chicago 2016, pp. 177–186.

Aghda S F and Bagheri V 2015 Evaluation of earthquake-induced landslides hazard zonation methods: A case study of Sarein, Iran, earthquake (1997); *Arab. J. Geosci.* **8(9)** 7207–7227.

Aghdam I N, Pradhan B and Panahi M 2017 Landslide susceptibility assessment using a novel hybrid model of statistical bivariate methods (FR and WOE) and adaptive neuro-fuzzy inference system (ANFIS) at southern Zagros Mountains in Iran; *Environ. Earth Sci.* **76(6)** 237.

Baeza C and Corominas J 2001 Assessment of shallow landslide susceptibility by means of multivariate statistical techniques. Earth Surface Processes and Landforms; *J. British Geomorphol. Res. Group* **26(12)** 1251–1263.

Barnard P L, Owen L A, Sharma M C and Finkel R C 2001 Natural and human-induced landsliding in the Garhwal Himalaya of northern India; *Geomorphology* **(1–2)** 21–35.

BIS 2016 Indian Standard, Criteria for earthquake resistance design of structures: Part 1: General Provisions and Buildings, Bureau of Indian Standards, New Delhi.

Bojadjieva J, Sheshov V and Bonnard C 2018 Hazard and risk assessment of earthquake-induced landslides – case study; *Landslides* **15(1)** 161–171.

Budimir M E A, Atkinson P M and Lewis H G 2015 A systematic review of landslide probability mapping using logistic regression; *Landslides* **12(3)** 419–436.

CartoDEM data 2017, https://bhuvan.nrsc.gov.in/bhuvan_links.php.

Champati R, Dimri S, Lakhera R C and Sati S 2007 Fuzzy-based method for landslide hazard assessment in active seismic zone of Himalaya; *Landslides* **4(2)** 101.

Chauhan S, Sharma M and Arora M K 2010 Landslide susceptibility zonation of the Chamoli region, Garhwal Himalayas, using logistic regression model; *Landslides* **7(4)** 411–423.

Chen W, Shahabi H, Zhang S, Khosravi K, Shirzadi A, Chapi K, Pham B, Zhang T, Zhang L, Chai H and Ma J 2018 Landslide susceptibility modeling based on GIS and novel bagging-based kernel logistic regression; *Appl. Sci.* **8(12)** 2540.

Chousianitis K, Del Gaudio V, Sabatakakis N, Kavoura K, Drakatos G, Bathrellos G D and Skilodimou H D 2016 Assessment of earthquake-induced landslide hazard in Greece: From Arias intensity to spatial distribution of slope resistance demand assessment of earthquake-induced landslide hazard in Greece; *Bull. Seismol. Soc. Am.* **106(1)** 174–188.

Chung C J and Fabbri A G 1999 Probabilistic prediction models for landslide hazard mapping; *Photogramm. Eng. Remote Sens.* **65(12)** 1389–1399.

Dai F C and Lee C F 2002 Landslide characteristics and slope instability modeling using GIS, Lantau Island, Hong Kong; *Geomorphology* **42(3–4)** 213–228.

Ding Q, Chen W and Hong H 2017 Application of frequency ratio, weights of evidence and evidential belief function models in landslide susceptibility mapping; *Geocarto. Int.* **32(6)** 619–639.

Fell R, Corominas J, Bonnard C, Cascini L, Leroi E and Savage W Z 2008 Guidelines for landslide susceptibility, hazard and risk zoning for land-use planning; *Engg. Geol.* **102(3–4)** 99–111.

Gaudio V, Pierri P and Wasowski J 2003 An approach to time-probabilistic evaluation of seismically induced landslide hazard; *Bull. Seismol. Soc. Am.* **93(2)** 557–569.

Gorum T, Gonencgil B, Gokceoglu C and Nefeslioglu H A 2008 Implementation of reconstructed geomorphologic units in landslide susceptibility mapping: The Melen Gorge (NW Turkey); *Nat. Hazards* **46(3)** 323–351.

Hungr O 2016 A review of landslide hazard and risk assessment methodology; In: *Landslides and Engineered Slopes. Experience, Theory and Practice;* CRC Press, Boca Raton, pp. 3–27.

James N and Sitharam T G 2014 Assessment of seismically induced landslide hazard for the State of Karnataka using GIS technique; *J. Indian Soc. Remote Sens.* **42(1)** 73–89.

Kanungo D P, Arora M K, Sarkar S and Gupta R P 2006 A comparative study of conventional, ANN black box, fuzzy and combined neural and fuzzy weighting procedures for

landslide susceptibility zonation in Darjeeling Himalayas; *Eng. Geol.* **85(3–4)** 347–366.

Kumar R and Anbalagan R 2019 Landslide susceptibility mapping of the Tehri reservoir rim area using the weights of evidence method; *J. Earth Syst. Sci.* **128(6)** 153.

Kundu S, Saha A K, Sharma D C and Pant C C 2013 Remote sensing and GIS based landslide susceptibility assessment using binary logistic regression model: A case study in the Ganeshganga Watershed, Himalayas; *J. Indian Soc. Remote Sens.* **41(3)** 697–709.

Landsat 8, Operational Land Imager (OLI) and Thermal Infrared Sensor (TIRS) data, https://www.usgs.gov/.

Lee S and Evangelista D G 2006 Earthquake-induced landslide-susceptibility mapping using an artificial neural network; *Nat. Hazard Earth Syst.* **6(5)** 687–695.

Lee S and Min K 2001 Statistical analysis of landslide susceptibility at Yongin, Korea; *Environ. Geol.* **40(9)** 1095–1113.

Lee C T, Huang C C, Lee J F, Pan K L, Lin M L and Dong J J 2008 Statistical approach to earthquake-induced landslide susceptibility; *Eng. Geol.* **100(1–2)** 43–58.

Liu J, Shi J, Wang T and Wu S 2018 Seismic landslide hazard assessment in the Tianshui area, China, based on scenario earthquakes; *Bull. Eng. Geol. Environ.* **77(3)** 1263–1272.

Miles S B and Keefer D K 2009 Evaluation of CAMEL-comprehensive areal model of earthquake-induced landslides; *Eng. Geol.* **104(1–2)** 1–15.

Nguyen V V, Pham B T, Vu B T, Prakash I, Jha S, Shahabi H, Shirzadi A, Ba D N, Kumar R, Chatterjee J M and Tien Bui D 2019 Hybrid machine learning approaches for landslide susceptibility modeling; *Forests* **10(2)** 157.

NRSC Report 2014 Evaluation of Indian National DEM (version 2) from Cartosat-1 data, National Remote Sensing Center, Hyderabad.

Pradhan B, Singh R P and Buchroithner M F 2006 Estimation of stress and its use in evaluation of landslide prone regions using remote sensing data; *Adv. Space Res.* **37(4)** 698–709.

Rajendran K, Rajendran C P, Jain S K, Murty C V and Arlekar J N 2000 The Chamoli earthquake, Garhwal Himalaya: Field observations and implications for seismic hazard; *Curr. Sci.* **78(1)** 45–51.

Refice A and Capolongo D 2002 Probabilistic modeling of uncertainties in earthquake-induced landslide hazard assessment; *Comput. Geosci.* **28(6)** 735–749.

Regmi N R, Giardino J R and Vitek J D 2010 Modeling susceptibility to landslides using the weight of evidence approach: Western Colorado, USA; *Geomorphology* **115(1–2)** 172–187.

Saha A K, Gupta R P, Sarkar I, Arora M K and Csaplovics E 2005 An approach for GIS-based statistical landslide susceptibility zonation-with a case study in the Himalayas; *Landslides* **2(1)** 61–69.

Sangeeta and Maheshwari B K 2018 Earthquake-induced landslide hazard assessment of Chamoli District, Uttarakhand, India using weighted overlay method; In: *16th European Conference on Earthquake Engineering* (ed.) Pitilakis K, Thessaloniki, Greece.

Sangeeta and Maheshwari B K 2019 Earthquake-Induced Landslide Hazard Assessment of Chamoli District, Uttarakhand Using Relative Frequency Ratio Method; *Indian Geotech. J.* **49(1)** 108–123.

Sarkar S and Kanungo D P 2004 An integrated approach for landslide susceptibility mapping using remote sensing and GIS; *Photogramm. Eng. Remote Sens.* **70(5)** 617–625.

Sarkar S, Kanungo D P and Sharma S 2015 Landslide hazard assessment in the upper Alaknanda valley of Indian Himalayas; *Geomat. Nat. Haz. Risk* **6(4)** 308–325.

Shrestha S, Kang T S and Choi J C 2018 Assessment of co-seismic landslide susceptibility using LR and ANCOVA in Barpak region, Nepal; *J. Earth Syst. Sci.* **127(3)** 38.

Shrikhande M, Rai D C, Naryan J and Das J 2000 The March 29, 1999 earthquake at Chamoli, India; In: *Proceedings of the Twelfth World Conference on Earthquake Engineering*, Upper Hutt, NZ: New Zealand Society for Earthquake Engineering, 8p.

Sinha B N, Varma R S and Paul D K 1975 Landslides in Darjeeling district (West Bengal) and adjacent areas; *Bull. Geol. Surv. India* **36(B)** 1–10.

Song Y, Gong J, Gao S, Wang D, Cui T, Li Y and Wei B 2012 Susceptibility assessment of earthquake-induced landslides using Bayesian network: A case study in Beichuan, China; *Comput. Geosci.* **42** 189–199.

Tanoli J I, Ningsheng C, Regmi A D and Jun L 2017 Spatial distribution analysis and susceptibility mapping of landslides triggered before and after Mw7.8 Gorkha earthquake along Upper Bhote Koshi, Nepal; *Arab. J. Geosci.* **10(13)** 277.

Umar Z, Pradhan B, Ahmad A, Jebur M N and Tehrany M S 2014 Earthquake-induced landslide susceptibility mapping using an integrated ensemble frequency ratio and logistic regression models in West Sumatera Province, Indonesia; *Catena* **118** 124–135.

Valdiya K S 1980 Geology of Kumaun lesser Himalaya. Wadia Institute of Himalayan Geology, Google Scholar, Dehradun, 291p.

Varnes D J 1984 *Landslide hazard zonation: A review of principles and practice*; United Nations Educations (UNESCO), ISBN: 92-3-101895-7.

Wang Q, Li W, Chen W and Bai H 2015 GIS-based assessment of landslide susceptibility using certainty factor and index of entropy models for the Qianyang County of Baoji city, China; *J. Earth Syst. Sci.* **124(7)** 1399–1415.

Wang X, Nie G and Wang S 2011 Ground motion acceleration criterion for judging landslide induced by the 2008 Wenchuan earthquake; *Acta Seismol. Sinica* **33(1)** 82–90.

Wu C 2016 Comparison and applicability of landslide susceptibility models based on landslide ratio-based logistic regression, frequency ratio, weight of evidence, and instability index methods in an extreme rainfall event; In: *EGU General Assembly Conference Abstracts* (vol. 18).

Corresponding editor: N V Chalapathi Rao